Structural link to precursor effects

R. Bindu,[1] Kalobaran Maiti,[1,*] S. Khalid,[2] and E. V. Sampathkumaran[1]
[1]*Department of Condensed Matter Physics and Materials Science, Tata Institute of Fundamental Research, Homi Bhabha Road, Colaba, Mumbai 400 005, India*
[2]*National Synchrotron Light Source, Brookhaven National Laboratory, Upton, New York 11973, USA*
(Received 9 January 2009; published 9 March 2009)

We investigate the origin of precursor effect associated to magnetic phase transitions in a quasi-one-dimensional system $Ca_3Co_2O_6$, employing extended x-ray absorption fine structure technique. Experimental results reveal unusual changes in the Co-O bond lengths in CoO_6 units nucleating at a temperature $T^\star$, where the precursor effect occurs. The corresponding Debye-Waller factors representing disorder effect exhibit anomalous evolution across $T^\star$. These results reveal a unique link between the local structural changes and the precursor effect that needs to be considered in the understanding of various phase transitions.

DOI: 10.1103/PhysRevB.79.094103 PACS number(s): 75.30.Kz, 61.05.cj, 61.50.Ks

I. INTRODUCTION

Observation of the signature of ground states at a temperature $T^\star$ higher than the phase transition temperature is known as precursor effects. Numerous studies evidenced precursor effect associated to superconducting transition,[1] magnetic transition,[2] etc. However, the origin of $T^\star$ is unclear. In this work, we have studied the temperature evolution of the local structural units CoO_6, responsible to determine the electronic properties in a quasi-one-dimensional system $Ca_3Co_2O_6$.

Recently, $Ca_3Co_2O_6$ has drawn great current interest due to many interesting properties exhibited by this system.[3–14] This compound forms in K_4CdCl_6 structure[7] (space group $R\bar{3}c$) as shown in Fig. 1. CoO_6 units form one-dimensional (Ising) chains (along the c axis), where Co appears alternately in octahedral (Oct) and trigonal prismatic (TP) crystal fields. Each chain is surrounded by six equally spaced chains forming a triangular lattice in the ab plane. This typical structure leads to a plethora of interesting properties involving geometrical frustration[7–14] unlike other one-dimensional systems.[15–19] Various studies[10–12] suggest intrachain ferromagnetic (FM) ordering at ~ 24 K and a complex transition at about 10 K.[11] At $T<24$ K, the magnitude of the magnetic moment along the chain is modulated.[3] Interestingly, a recent Mössbauer study on $Ca_{2.9}Eu_{0.1}Co_2O_6$ showed the signature of magnetic order at ~ 80 K revealing precursor effect prior to the magnetic transition.[20] Thus, this compound is ideally suited to address the issue.

Several contrasting models are proposed to explain the magnetic interactions in this system. For example, one model suggests that Co-Co direct exchange interaction plays a dominant role in the intrachain FM coupling[21] and the interchain antiferromagnetic (AFM) coupling was attributed to the Co-O-O-Co supersuperexchange interaction. The other model[4] suggests a role of the oxygen $2p$ holes arising due to the O $2p$-Co $3d$ hybridization in determining the intrachain FM interactions. Since the hybridization parameters are essentially determined by the associated bond lengths, bond angles etc., it is important to probe the evolution of the local structural parameters to address the above issue. In this paper, we report our results of the investigations of the evolution of the CoO_6 polyhedra as a function of temperature employing Co K-edge x-ray absorption spectroscopy (XAS) in the extended energy range. We observe a link between the structural parameters and the precursor effect.

II. EXPERIMENTAL

The sample was prepared by conventional solid-state route and characterized by powder x-ray diffraction (XRD).[11] The XRD pattern confirmed single phase. The analysis of the diffraction peaks at room temperature indicates rhombohedral structure with $R\bar{3}c$ space group.

Temperature-dependent Co K-edge XAS measurements were carried out at beamline X-18B at the National Synchrotron Light Source, Brookhaven National Laboratory using closed cycle helium cryostat. The storage ring has electron energy of 2.8 GeV and current of 300 mA. The beamline uses a Si(111) channel cut monochromator, which is water cooled by gravitational system to minimize any vibrations and noise in the spectra. The beamline vacuum is in the range of 10^{-9} Torr and there are no mirrors or any other optics between the x-ray source and the monochromator. The monochromator is placed 18 m away from the source, so that the horizontal acceptance angle of the beam at the mono-

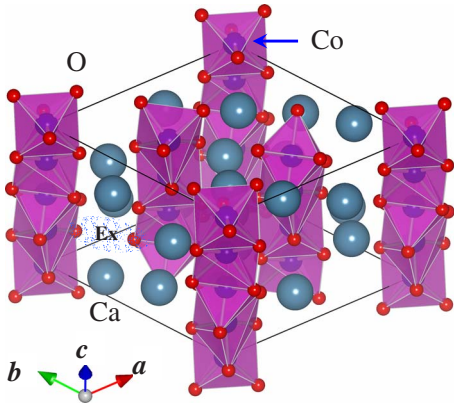

FIG. 1. (Color online) Crystal structure of $Ca_3Co_2O_6$. The shaded area marked Ex indicate the interchain O-O distance.

chromator is 1 mrad. The vertical slit size used in this experiment was 1 mm at a distance of 17.5 m from the source, corresponding to an energy resolution of 0.8 eV at the Co *K* edge. As we have used Si(111) crystal monochromator, the second harmonic was not present, the third and higher harmonics were suppressed by detuning the second crystal. A picomotor operated through a piezo does the detuning and it was done to cut down the initial flux by 35%. At this detuning, less than 0.5% of harmonics were left in the outgoing x-ray beam.

Oxford instruments ionization chambers were used to measure the incident (I_0) and the transmitted beams (I_t). These are sealed ion chambers, where a mixture of inert gases was used for the optimum linearity of the detector and for best signal to noise ratio. At Co *K* edge of 7709 eV, the gas mixture used in I_0 chamber was 70% He and 30% N_2, absorbing 14.5% of incident photons. The gas mixture in I_t chamber was 100% N_2, absorbing 40% of remaining photons after the sample. The positive offsets of the ion chambers were taken with the x-ray beam shutters closed and they were subtracted from the data. This way the electronic noise was eliminated. The photon flux was in the range of 10^{10} photons/s and, therefore, the statistical noise is within 0.001%. The settling time of the monochromator was 0.5 s. All the mechanical vibrations of the monochromators were fully damped before the data collection started for at least 2 s at each energy point in the scan. The electronic, mechanical, and statistical noises of the data were minimized by taking all the above three precautions into account and the signal to background value as measured was better than 0.005%, which is much superior than any fine extended x-ray absorption fine structure (EXAFS) features.

For calibration purpose, standard Co foil was used between I_t and another gas flow ion chamber I_{ref} and no energy shift was observed in the reference spectra between the series of the sample scans collected at different temperatures. At beamline X-18B, we use a Heidenhain optical encoder attached to the axis of rotation of the monochromator and it reads the absolute Bragg angle corresponding to the energy of the Si(111) crystal. The pulse generating module E500 of CAMAC keeps sending the pulses unless the correct absolute energy is reached. Also during data analysis (using ATHENA software) all the spectra are matched with the reference spectra for absolute energy. This way even if there is an energy drift, it is corrected. The energy drift is mechanically corrected by using optical encoder and in addition during analysis using ATHENA program.

To record the spectra, the powdered samples sieved through a 400 mesh were spread uniformly on an adhesive tape and four layers of this tape were used to minimize the pinhole and brick effects. The pinhole corresponds to absence of the sample material and the brick corresponds to increased thickness of the absorber material in the path of the incident radiation. The value of $\mu x = \ln(I_0/I_t)$ would thus be different in the pinhole and the brick areas of the sample: for the former it would be almost zero and for the latter it would be very large. Such inhomogeneity distorts the recorded spectra.

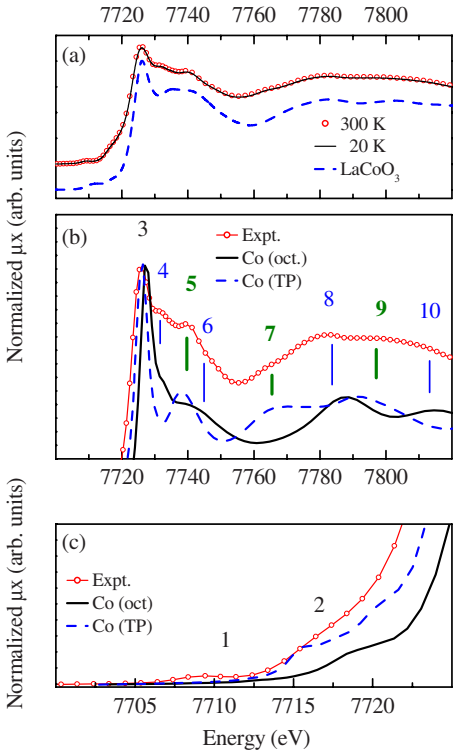

FIG. 2. (Color online) (a) XANES spectra of $Ca_3Co_2O_6$ at 300 and 20 K compared with the room-temperature spectrum of $LaCoO_3$. (b) Experimental spectrum in the postedge region is compared with the calculated spectra considering the absorbing center at octahedral (solid line) and trigonal prismatic (dashed line) environments. (c) Pre-edge region is compared with the calculated spectra.

III. RESULTS AND DISCUSSIONS

A. X-ray absorption near-edge structure

The Co *K*-edge x-ray absorption near-edge structure (XANES) spectra are shown in Fig. 2(a). The room-temperature spectrum of $LaCoO_3$ is also shown by dashed line in the figure. The features in this energy range are found to be less sensitive to the temperature. This is shown by superimposing the 300 and 20 K spectra in the figure. The spectra collected at all the intermediate temperatures are essentially identical to the ones shown here. These features are somewhat different from those in $LaCoO_3$. Evidently, the energy position of the Co *K* edge observed in $Ca_3Co_2O_6$ is very close to that in $LaCoO_3$; this suggests that the valency of Co in $Ca_3Co_2O_6$ is three for Co at both octahedral and trigonal prismatic sites.[22–25]

In order to investigate the origin of spectral features, the XANES spectra were calculated using multiple-scattering scheme of FEFF 8.2 code[26] considering Co in both Oct and TP sites. The calculated spectra for the pre-edge peaks 1 and 2 shown in Fig. 2(c) exhibit good description of the experimental spectra.[27] In a recent study, it was proposed that pre-edge structures may appear due to the quadrupolar transitions and/or nonlocally screened dipolar transitions.[28] In our study, peak 2 could be captured without considering nonlocal screening effect and the quadrupole contribution in the cal-

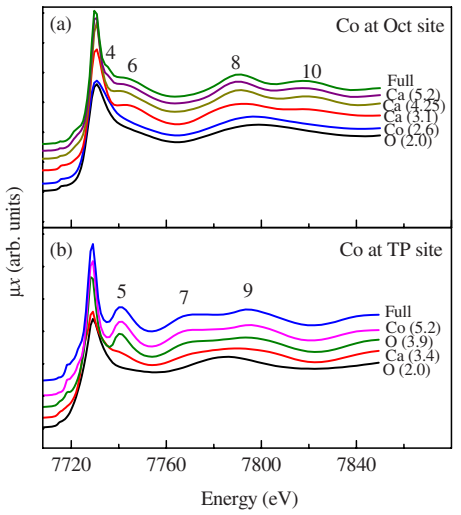

FIG. 3. (Color online) Calculated XANES spectra centered at Oct and TP sites. The features due to various contributions are shown explicitly. The numbers in the parenthesis represent the distance in Å from the scattering center. The term "full" refers to consideration of all the contributions.

culation; this peak can be attributed to be due to *pd* mixing. However, peak 1 appears only when quadrupole contribution in addition to the dipole term is included as also observed in other systems.[28]

In Fig. 2(b), we show the postedge region. The evolution of the calculated results due to various contributions is shown in Fig. 3. From the calculated spectra, it is evident that features 4, 6, 8, and 10 correspond to the signals from octahedral Co as also seen in $LaCoO_3$. These features appear when neighboring Ca ions placed at about 3 Å away from the octahedral site are considered. When next-nearest neighbors are added into the cluster, these features become sharper. In the calculations considering Co at TP site, feature 5 is seen to develop when the neighboring Ca ions at 3.35 Å are included in the calculation. This feature becomes more prominent and distinct signature of features 7 and 9 start to develop when the contribution of neighboring oxygen ions at about 3.87 Å away from TP site is invoked. All the above results reveal four important conclusions: (a) Co at both the lattice sites are trivalent, (b) *pd* mixing may be significant, (c) the signature of all the features in the postedge experimental spectra could be simulated within mean-field descriptions, and (d) within the limitation of the present study, the influence of temperature is not visible in this energy range.

B. EXAFS

Now, we turn to the EXAFS region (energy range up to 8500 eV) in the absorption spectra. A typical spectrum is shown in the inset of Fig. 4(a). The fine structures in the EXAFS region shown by rescaling the spectrum in the extended energy range appear due to the interference of the outgoing photoelectron waves and the backscattered waves (from the neighboring atoms).

EXAFS analysis was carried out by using the ARTEMIS and ATHENA programs[29] using the IFEFFIT data analysis

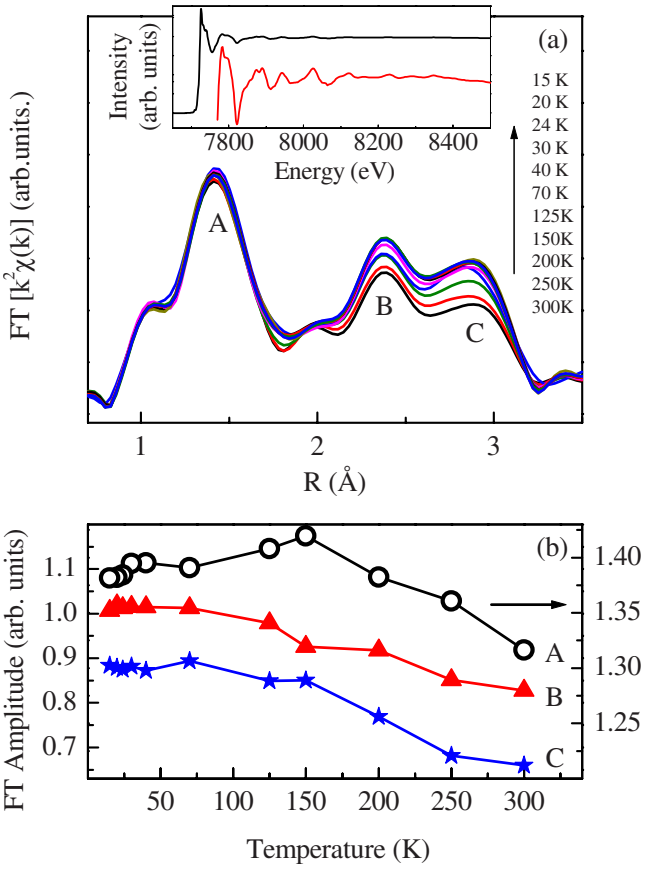

FIG. 4. (Color online) (a) Fourier transform (FT) of $k^2\chi(k)$ representing various bond lengths at different temperatures. The inset shows a typical x-ray absorption spectrum. For clarity, the fine structures in the EXAFS region are shown by rescaling. (b) The temperature dependence of peaks A–C in the FT amplitude shown in (a).

package[30] following the standard procedure.[31] The threshold energy E_0 was chosen by taking the inflection point around the absorption edge region of the experimental spectrum. After background subtraction, the absorption coefficient $\mu(E)$ was converted to $\mu(k)$, where

$$k = [2m(E - E_0)/\hbar^2]^{1/2}$$

is the magnitude of the wave vector of the ejected photoelectron. The XAFS oscillation $\chi(k)$ is defined as

$$\chi(k) = (\mu - \mu_0)/\mu_0,$$

where μ_0 is the embedded atom absorption coefficient. The Fourier transform to the r space was taken in the k range of 2.5–14.55 $Å^{-1}$ by Fourier transforming $k^2\chi(k)$ with a Kaiser-Bessel window function.

The calculated Fourier transform of $k^2\chi(k)$ is shown in Fig. 4(a). These spectra are uncorrected for the central and backscattered phase shifts. The first coordination shell marked A corresponds to Co_{Oct}-O and Co_{TP}-O bond distances. Peaks B and C represent intrachain Co_{Oct}-Co_{TP}, Co_{Oct}-Ca, and multiple-scattering paths (Co_{Oct}-O-O, Co_{Oct}-O-Co_{TP}) and Co_{TP}-Ca, respectively. On lowering the temperature, the Fourier-transform amplitude of

features B and C increases as shown in Fig. 4(b) and becomes almost flat below about 75 K. The change in amplitude of feature A exhibits anomalous behavior with temperature.

The EXAFS function $\chi(k)$ can be expressed as

$$\chi(k) = S_0^2 \sum_j \frac{N_j F_j(k)}{2kR_j^2} \exp(-2k^2\sigma_j^2) \exp(-2R_j/\lambda) \times \sin[2kR_j + \phi_j(k)],$$

where N_j is the number of atoms in the jth shell placed at an average distance R_j from the scattering center, $F_j(k)$ is the backscattering amplitude, σ_j^2 is the Debye-Waller factor, λ is the photoelectron mean-free path, S_0^2 is a constant which takes into account the many-body effects, and $\phi_j(k)$ corresponds to effective scattering phase shift. Clearly, the peak intensity in Fig. 4 is a sensitive function of R_j and σ^2. Thus, the temperature-induced changes manifested in the figure indicate significant reorganization or modification of the local structure parameters as one approaches the magnetic transitions.

In order to estimate the local structural parameters, the theoretical model for EXAFS analysis was constructed with the FEFF 6.01 code[26,32] using the crystallographic positions of $Ca_3Co_2O_6$. In the case of first coordination shell, the initial structural parameters were obtained from room-temperature XRD data reported in the literature.[7] At room temperature, the average Co-O bond lengths in the octahedral environment is ~1.92 Å and in the trigonal prismatic environment, it is 2.06 Å. The bond-length difference of 0.14 Å is higher than the experimental resolution $\Delta R = \pi/2(k_{max} - k_{min})$ for the k range used for fitting. We have modeled the first coordination shell with six Co_{Oct}-O bonds and Co_{TP}-O bonds. The first shell fitting was done in the Fourier-filtered k space in the range of 1.13–1.77 Å. During the course of fitting, the number of free parameters and their correlation were minimized by suitable choice of constraints. For example, the number of nearest neighbors was kept fixed as per the choice of the model structure and only bond lengths and corresponding Debye-Waller factors were refined to reduce the number of correlated parameters. Usually, a fit was considered to be good if the goodness of the fit given by R factor is less than 0.02.[30]

The higher shell fitting was carried out to get the information about Co_{Oct}-Co_{TP} and Co_{Oct}-Ca/Co_{TP}-Ca bond lengths. We have considered average bond lengths in each shell in order to reduce the number of variable parameters and corresponding paths, thereby reducing the uncertainty of the parameters. The room-temperature and 40-K XRD data were used as starting parameters. It was found that for $T < 150$ K, the R factor improved drastically when the starting parameters were taken from the 40-K XRD data. Typical R factors obtained for the first coordination and higher shells are 0.004 and 0.007, respectively. The overall many-body reduction factor S_0^2 arising from the overlap contribution of the passive electrons was around 0.7–0.9 and it was not very sensitive to the chemical environment. We have chosen S_0^2 to be 0.8, which provided the best fit.

A typical set of fits is shown in Fig. 5. It is evident that the

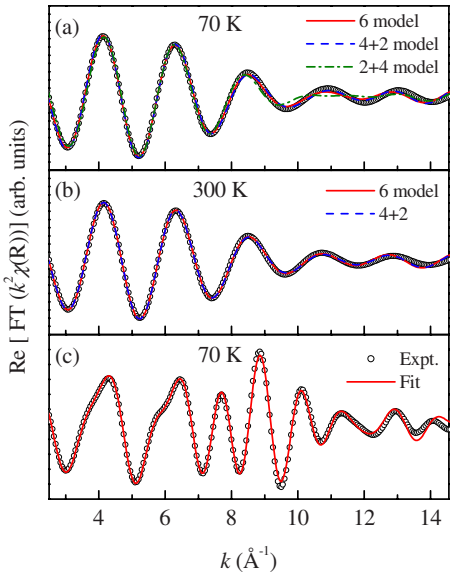

FIG. 5. (Color online) Typical fits obtained for first coordination shell at (a) 70 K and (b) 300 K. (c) The fit at 70 K for the higher coordination shell.

fits are very good for both the first coordination shell and higher coordination shell at different temperatures. In the case of first coordination shell fitting, we have verified the fitting parameters considering all six Co-O bond lengths equal (6 model), four short and two long Co-O bond lengths (4+2 model), and four long and two short Co-O bond lengths (2+4 model) around the octahedral site. We observe in Fig. 5 that the 6 model and 4+2 model provide very similar results and close to the experimental data. The results for the 2+4 model are significantly different from experimental data. This provides additional confidence in the consideration of average bond lengths for the fittings. Our estimations are consistent with the available XRD data.[7]

The estimated bond distances and the Debye-Waller factors are shown in Figs. 6 and 7. On reducing the temperature, the Co-Ca distances and corresponding σ^2 gradually decrease as expected due to thermal contractions. Co_{Oct}-Co_{TP} distance does not exhibit significant change with temperature.

The changes in the Co_{Oct}-O and Co_{TP}-O bond distances and corresponding σ^2 are shown in Fig. 7. Evidently, there are four distinct temperature regions visible in the figure, which could be responsible for different temperature behaviors of resistivity.[9,33] Region I comprises the temperature range of 300–150 K, where the Co-O bond length and σ^2 marginally decrease with the decrease in temperature (thermal effect). In the temperature range of 150–70 K (region II), σ^2 exhibits anomalous behavior. While Co-O bond length decreases rapidly, σ^2 for Co_{Oct}-O bond increases with the decrease in temperature, in contrast to the expected trend, suggesting significant change in corresponding local electronic structure. This can be explained as follows. The octahedral crystal field around the Co_{Oct} site splits the d bands into t_{2g} and e_g bands. Co_{Oct} being in the low-spin state has all the t_{2g} levels almost filled and the e_g levels closed to empty. However, due to finite Co $3d$-O $2p$ covalency, the e_g band is

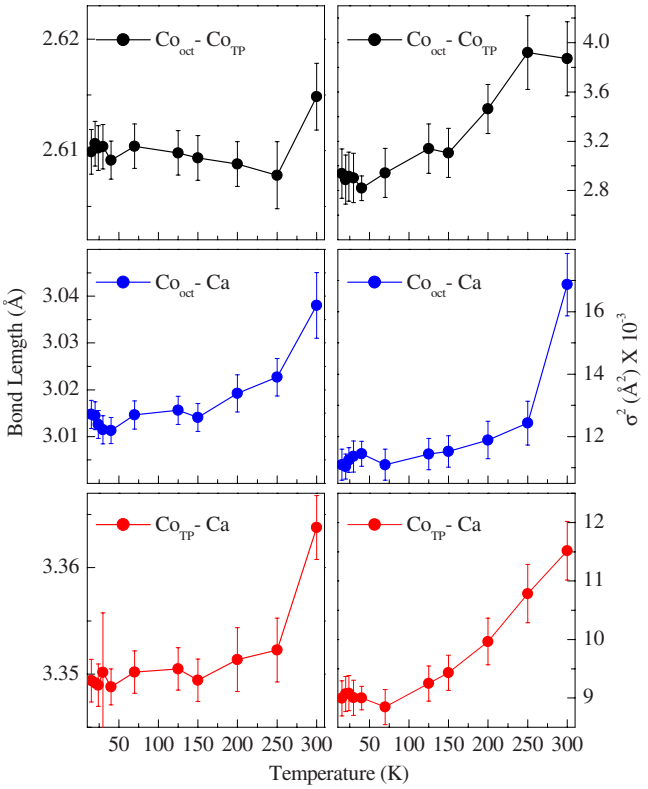

FIG. 6. (Color online) Bond lengths and the Debye-Waller factors σ^2 corresponding to Co_{Oct}-Co_{TP}, Co_{Oct}-Ca, and Co_{TP}-Ca bonds are plotted as functions of temperature.

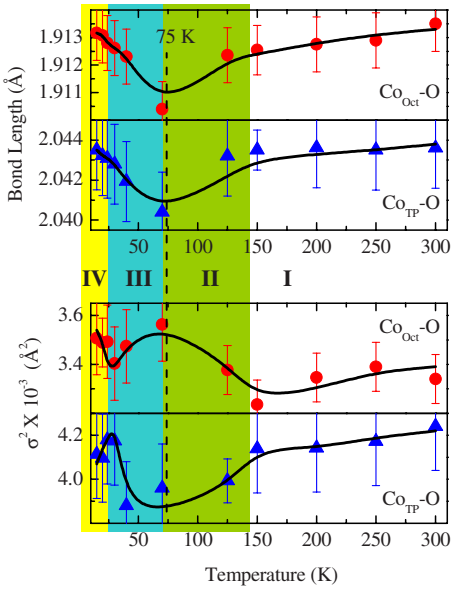

FIG. 7. (Color online) The temperature evolution of Co_{Oct}-O and Co_{TP}-O bond lengths and corresponding Debye-Waller factors are shown exhibiting signature of three distinct phases.

marginally filled leading to finite spin moment centered at the Co_{Oct} sites.[4] With the decrease in the Co_{Oct}-O bond lengths with temperature, the Co_{Oct} 3*d*-O 2*p* hybridization increases. Such effect will enhance the Co 3*d*-O 2*p* covalency, which may lead to significant occupation of the e_g bands. This makes the CoO_6 octahedra Jahn-Teller effect active leading to an enhancement of the distribution of Co_{Oct}-O bond lengths (σ^2 will increase).

In regime III (75– ~24 K), both the Co-O bond lengths increase indicating the onset of a stronger competing force that overcomes the thermal contraction. Such an enhancement in the bond length (negative expansion coefficient) nucleating at a temperature close to the critical temperature for precursor effect is interesting.[20] Here, σ^2 for Co_{Oct}-O bond reduces and that for Co_{TP}-O bond enhances sharply. Enhancement in Co_{TP}-O bond length in this region makes the bonds softer and would normally enhance σ^2. However, the Co_{Oct}-O case is opposite indicating stiffening of the bonds, although there is an enhancement in the bond length.

In region IV ($T<24$ K), all the Co-O bond lengths increase rapidly. The FM chains are separated by O and Ca ions. Since the Co_{Oct}-Co_{TP} distance remains almost unchanged, the increase in the Co-O bonds leads to an expansion of the CoO_6 units in the *ab* plane. Thus, the interchain O-O separation as shown by shaded area (marked "Ex") in Fig. 1 will decrease. This will help to enhance interchain antiferromagnetic coupling via Co-O-O-Co supersuperexchange interactions and makes its contribution significant.[21,34] The values of σ^2 exhibit extrema indicating significant modification of the disorder effect.

The above results establish that the Co 3*d*-O 2*p* hybridization and the holes in the O 2*p* bands play the major role in determining various magnetic orderings and the other electronic properties. Therefore, the key to various phase transition lies primarily in the local structural parameters. Needless to state that the insensitivity of the Co_{Oct}-Co_{TP} bond length to the temperature indicates that the sensitivity of the Co-Co direct exchange coupling to the intrachain long range order is not significant.

IV. CONCLUSIONS

In summary, we have studied the evolution of the local structural parameters across the magnetic phase transition employing EXAFS technique. These results provide a direct observation of anomalous change in the structural parameters that nucleates in the vicinity of the critical temperature for the precursor effect revealing a paradigm linking the precursor effect to the local structural changes. This is very interesting in the context of understanding precursor effect associated to various phase transitions. We hope that our results will provide enough incentive to the groups around the world to look into this in more detail using various other techniques.

*Corresponding author; kbmaiti@tifr.res.in

[1] A. Kanigel, M. R. Norman, M. Randeria, U. Chatterjee, S. Souma, A. Kaminski, H. M. Fretwell, S. Rosenhranz, M. Shi, T. Sato, T. Takahashi, Z. Z. Li, H. Raffy, K. Kadowaki, D. Hinks, L. Ozyuzer, and J. C. Campuzano, Nat. Phys. **2**, 447 (2006).

[2] N. Mannella, W. L. Yang, X. J. Zhou, H. Zheng, J. F. Mitchell, J. Zaanen, T. P. Devereaux, N. Nagaosa, Z. Hussain, and Z.-X. Shen, Nature (London) **438**, 474 (2005).

[3] S. Agrestini, L. C. Chapon, A. Daoud-Aladine, J. Schefer, A. Gukasov, C. Mazzoli, M. R. Lees, and O. A. Petrenko, Phys. Rev. Lett. **101**, 097207 (2008); S. Agrestini, C. Mazzoli, A. Bombardi, and M. R. Lees, Phys. Rev. B. **77**, 140403(R) (2008).

[4] Hua Wu, M. W. Haverkort, Z. Hu, D. I. Khomskii, and L. H. Tjeng, Phys. Rev. Lett. **95**, 186401 (2005).

[5] Y. B. Kudasov, Phys. Rev. Lett. **96**, 027212 (2006).

[6] A. Bombardi, C. Mazzoli, S. Agrestini, and M. R. Lees, Phys. Rev. B **78**, 100406(R) (2008).

[7] H. Fjellvåg, E. Gulbrandsen, S. Aasland, A. Olsen, and B. C. Hauback, J. Solid State Chem. **124**, 190 (1996).

[8] H. Kageyama, K. Yoshimura, K. Kosuge, H. Mitamura, and T. Goto, J. Phys. Soc. Jpn. **66**, 1607 (1997).

[9] B. Raquet, M. N. Baibich, J. M. Broto, H. Rakoto, S. Lambert, and A. Maignan, Phys. Rev. B **65**, 104442 (2002).

[10] S. Aasland, H. Fjellvåg, and B. Hauback, Solid State Commun. **101**, 187 (1997).

[11] S. Rayaprol, K. Sengupta, and E. V. Sampathkumaran, Solid State Commun. **128**, 79 (2003); E. V. Sampathkumaran, Z. Hiroi, S. Rayaprol, and Y. Uwatoko, J. Magn. Magn. Mater. **284**, L7 (2004).

[12] V. Hardy, S. Lambert, M. R. Lees, and D. McK. Paul, Phys. Rev. B **68**, 014424 (2003).

[13] J. Sugiyama, H. Nozaki, J. H. Brewer, E. J. Ansaldo, T. Takami, H. Ikuta, and U. Mizutani, Phys. Rev. B **72**, 064418 (2005).

[14] I. Matsubara, R. Funahashi, T. Takeuchi, S. Sodeoka, T. Shimizu, and K. O. Ueno, Appl. Phys. Lett. **78**, 3627 (2001).

[15] P. Gambardella, A. Dallmeyer, K. Maiti, M. C. Malagoli, W. Eberhardt, K. Kern, and C. Carbone, Nature (London) **416**, 301 (2002).

[16] K. Maiti and D. D. Sarma, Phys. Rev. B **58**, 9746 (1998).

[17] K. Maiti, D. D. Sarma, T. Mizokawa, and A. Fujimori, Europhys. Lett. **37**, 359 (1997); Phys. Rev. B **57**, 1572 (1998).

[18] K. Maiti, P. Mahadevan, and D. D. Sarma, Phys. Rev. B **59**, 12457 (1999).

[19] K. Maiti, R. S. Singh, V. R. R. Medicherla, S. Rayaprol, and E. V. Sampathkumaran, Phys. Rev. Lett. **95**, 016404 (2005).

[20] P. L. Paulose, Niharika Mohapatra, and E. V. Sampathkumaran, Phys. Rev. B **77**, 172403 (2008).

[21] R. Fresard, C. Laschinger, T. Kopp, and V. Eyert, Phys. Rev. B **69**, 140405(R) (2004).

[22] E. V. Sampathkumaran, N. Fujiwara, S. Rayaprol, P. K. Madhu, and Y. Uwatoko, Phys. Rev. B **70**, 014437 (2004).

[23] M.-H. Whangbo, D. Dai, H.-J. Koo, and S. Jobic, Solid State Commun. **125**, 413 (2003).

[24] V. Eyert, C. Laschinger, T. Kopp, and R. Frésard, Chem. Phys. Lett. **385**, 249 (2004).

[25] T. Burnus, Z. Hu, M. W. Haverkort, J. C. Cezar, D. Flahaut, V. Hardy, A. Maignan, N. B. Brookes, A. Tanaka, H. H. Hsieh, H.-J. Lin, C. T. Chen, and L. H. Tjeng, Phys. Rev. B **74**, 245111 (2006).

[26] A. L. Ankudinov, B. Ravel, J. J. Rehr, and S. D. Conradson, Phys. Rev. B **58**, 7565 (1998).

[27] Features 1 and 2 in the calculated spectra appear about 5 eV higher in energy compared to the experimental spectra. This energy difference presumably indicates the importance of electron-electron Coulomb repulsion, which is not considered in these calculations. This energy shift is close to the observed Coulomb energy U ($\sim$5 eV) (Ref. 4).

[28] G. Vankó, F. M. F. de Groot, S. Huotari, R. J. Cava, T. Lorenz, and M. Reuther, arXiv:0802.2744 (unpublished).

[29] B. Ravel and M. Newville, J. Synchrotron Radiat. **12**, 537 (2005).

[30] M. Newville, J. Synchrotron Radiat. **8**, 322 (2001).

[31] *X-ray Absorption: Principles, Applications, Techniques of EXAFS, SEXAFS and XANES*, edited by D. C. Konningsberger and R. Prins (Wiley, New York, 1988).

[32] S. I. Zabinsky, J. J. Rehr, A. Ankudinov, R. C. Albers, and M. J. Eller, Phys. Rev. B **52**, 2995 (1995).

[33] J. Kurkijärvi, Phys. Rev. B **8**, 922 (1973).

[34] J. B. Goodenough, *Magnetism and the Chemical Bond* (Interscience, New York, 1963).